Short-Circuit Modeling of DFIG-based WTG in Sequence Domain Considering Various Fault-Ride-Through Requirements and Solutions

Yuanzhu Chang, *Member, IEEE*, Ilhan Kocar, *Senior Member, IEEE*, Evangelos Farantatos, *Senior Member, IEEE*, Aboutaleb Haddadi, *Senior Member, IEEE*, and Manish Patel, *Senior Member, IEEE*

***Abstract*--The doubly fed induction generator (DFIG) based wind turbine generator (WTG) can activate different fault ride through (FRT) control schemes and circuits to comply with various grid code or utility interconnection requirements. These FRT solutions play a key role in the resulting fault current of the DFIG-based WTG as well as the voltages and currents distributed in faulted networks. This paper accounts for their impact by proposing a new generic sequence domain model of the DFIG-based WTG for static short circuit calculations. In this paper, the FRT configurations are classified into three types. The proposed model first calculates the positive- and negative-sequence current phasors under the specified FRT control. Then based on the control, the desired currents and voltages are calculated by explicit equations to determine whether the crowbar could operate during FRT operation. By comparing with detailed electromagnetic transient (EMT) simulations using an EPRI benchmark system, the proposed model, incorporated into an iterative steady state solver, is shown to be accurate to calculate voltage and current phasors in an efficient manner. The proposed model provides a rapid tool for short circuit computations and protective relaying studies considering various grid code requirements and FRT implementations.**

***Index Terms*—Doubly fed induction generator (DFIG), short circuit, wind turbine generator, protection systems.**

I. Introduction

UNLIKE full-size converter (FSC) based wind turbine generators (WTGs), also referred to as Type-IV WTGs, the doubly fed induction generator (DFIG) based WTG, also referred to as Type-III WTG, uses partially sized converters and thus has to enable special control and protection strategies to ride through power system faults and to comply with various grid code or utility interconnection requirements [1]-[2]. The fault behavior of DFIG-based WTGs is more complex than that of conventional synchronous generators (SGs) [3] and varies when adjusted to comply with grid codes [4]. This different fault current response introduces technical challenges in short circuit analysis leading to maloperation and miscoordination [5]-[8] when assumed to behave like a conventional source. The development of accurate models for the DFIG-based WTG is a critical step to perform accurate short circuit studies in modern power systems.

Detailed models developed in electromagnetic transient-type (EMT-type) programs and real-time simulators [9]-[11] allow retaining the circuit topology and control schemes of the DFIG-based WTG. Simplified root-mean-square (RMS) models of DFIG-based WTGs are also proposed for transient stability and planning studies [12]-[14]. Even though the detailed EMT models can fully consider the fault ride through (FRT) strategies, the computational time is demanding and not practical for routine protective relaying studies performed by protection engineers particularly in real network cases with large-scale integration of renewables. On the other hand, the existing electromechanical models consider positive-sequence quantities for transient stability studies. For the computation of the fundamental-frequency components of voltages and currents in steady state following symmetrical and unsymmetrical faults, the DFIG-based WTG is simply replaced with voltage source behind fixed impedance or fixed current source according to the IEC Standard that is typically available as a solver option in professional short circuit packages [15]. This way, the short circuit computation becomes a linear problem, however, the results are not accurate since the impact of the FRT control schemes and circuits is neglected [16]-[17]. By considering the converter control during FRT, new phasor domain models are proposed to represent the DFIG-based WTG with controlled current sources [18]-[19]. To deal with the nonlinearity introduced by the control schemes, iterative solvers in steady state are proposed to obtain efficient and accurate solutions for protection studies [20]-[21]. However, the existing phasor models of the DFIG-based WTG do not fully consider the variety of FRT control schemes in different grid code requirements and WTG onboard protection. Moreover, the voltage control capability of the rotor side converter (RSC) has been ignored. These gaps lead to a need for development of accurate short circuit model of DFIG WTG capable of adequately representing typical grid code-specific FRT functionalities, which has been addressed in this paper.

Certain grid codes require the DFIG-based WTG to remain connected to the grid and provide additional positive-sequence reactive current (I1R) whether the fault is balanced or not [22]-[23]. This can be achieved with a basic control implementation

Y. Chang and I. Kocar are with the Hong Kong Polytechnic University, Hong Kong SAR, China (e-mail: yuanzhu.chang@polyu.edu.hk; ilhan.kocar@polyu.edu.hk).

E. Farantatos and A. Haddadi are with the Electric Power Research Institute (EPRI), Palo Alto, USA (e-mails: efarantatos@epri.com; ahaddadi@epri.com).

M. Patel is with the Southern Company Services, Forest Park, Georgia, USA (e-mail: mpatel@southernco.com).

regulating the positive-sequence quantities of the DFIG with a balanced positive-sequence control scheme (denoted as BPSC in this paper) [24]. In addition to that, in order to eliminate the electromagnetic torque (Tem) oscillation of DFIG caused by voltage unbalance, a number of control schemes have been developed by employing an additional negative-sequence control for the RSC [25]-[26]. A typical implementation of this FRT control scheme denoted by PNSC-Tem (positive and negative sequence control for electromagnetic torque) is considered in this paper for comparison purposes. Recent grid codes, such as German and Chinese grid codes, and the IEEE Std. 2800 introduce additional requirements on the negative-sequence reactive current (I2R) [27]-[29] in addition to I1R. A coordinated control strategy has been proposed in [30] denoted by PNSC-I12R (flexible I1R and I2R control) to comply with the requirement on the additional I2R. This paper demonstrates that under these three different types of FRT control schemes, DFIG-based WTGs contribute different fault currents to power grid.

Note that, DFIG-based WTG's converters are rated to convert the slip power (typically 30% of the rated power) [31]. Although some advanced transient control schemes can enhance the FRT ability of the DFIG-based WTG and help avoiding crowbar operation [32]-[33], under severe voltage dips and unbalance, converters may face overvoltage or overcurrent that do not decay [29]. To protect the converters, the FRT control schemes mentioned above will need to be interrupted by crowbar protection. Thus, crowbar circuit as well as its operating criterion should be accounted for in short circuit computations as will be addressed in this paper.

The original contribution of this paper is a new generic sequence domain model for DFIG-based WTG for short circuit calculations in steady state. The proposed sequence-domain model is incorporated into a modified-augmented-nodal-analysis (MANA) based iterative solver [34]-[35]. The accuracy is validated with EMTP simulations using detailed EMT-type models. Compared with the existing phasor models, the proposed model considers the typical FRT implementations and allows modeling with respect to recent grid codes.

The rest of the paper is organized as follows. Section II presents the framework of the proposed model. Section III deduces mathematical equations of DFIG-based WTG's current phasors in the positive- and negative-sequence systems and explains the calculation process. In Section IV, the desired voltages and currents by the FRT control are estimated to identify the operating criteria of the crowbar circuit. Section V validates the proposed model in terms of accuracy and efficiency. The phasor characteristics of the DFIG-based WTG is also discussed. Finally, conclusions are drawn in Section VI.

II. Proposed Sequence-Domain Short-Circuit Model

This section integrates the DFIG equations and control interfaces into the positive- and negative-sequence networks for the purpose of power system fault analysis. The framework of the proposed sequence-domain model is introduced.

A. DFIG in Positive- and Negative-Sequence Networks

The schematic of a DFIG-based WTG is shown in Fig. 1. Since the zero-sequence components are blocked by the typically Delta-connected wind park (WP) transformer, positive- and negative-sequence components of the voltages, currents, and flux linkages of the DFIG are the focus. Under the given current direction, the steady-state equations of the DFIG have been detailed with the space vectors in [30] and [36].

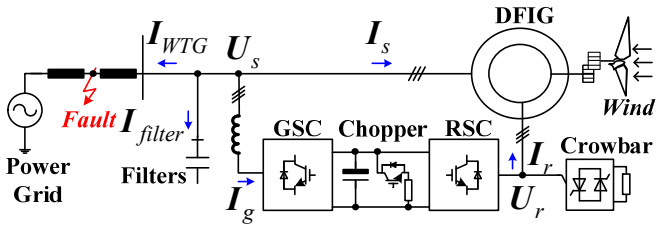

Fig. 1. Schematic of a DFIG-based WTG with the given current direction.

The positive-sequence equations are

$$\begin{aligned} \boldsymbol{U}_{s+}^{dq+} &\cong j\omega_1 \boldsymbol{\psi}_{s+}^{dq+} = j\omega_1 (L_s \boldsymbol{I}_{s+}^{dq+} + L_m \boldsymbol{I}_{r+}^{dq+}) \\ \boldsymbol{U}_{r+}^{dq+} / s &\cong j\omega_1 \boldsymbol{\psi}_{r+}^{dq+} = j\omega_1 (L_m \boldsymbol{I}_{s+}^{dq+} + L_r \boldsymbol{I}_{r+}^{dq+}) \end{aligned} \tag{1}$$

and the negative-sequence equations of the DFIG are

$$\begin{aligned} \boldsymbol{U}_{s-}^{dq-} &\cong -j\omega_1 \boldsymbol{\psi}_{s-}^{dq-} = -j\omega_1 (L_s \boldsymbol{I}_{s-}^{dq-} + L_m \boldsymbol{I}_{r-}^{dq-}) \\ \boldsymbol{U}_{r-}^{dq-} / (2-s) &\cong -j\omega_1 \boldsymbol{\psi}_{r-}^{dq-} = -j\omega_1 (L_m \boldsymbol{I}_{s-}^{dq-} + L_r \boldsymbol{I}_{r-}^{dq-}) \end{aligned} \tag{2}$$

where

$$s = (\omega_1 - \omega_r) / \omega_1 \tag{3}$$

where U, I and ψ stand for voltage, current and flux linkage, respectively. Space vectors are represented in italic and bold font. L_s, L_r and L_m stand for the stator inductance, rotor inductance, and magnetizing inductance of the DFIG, respectively. s stands for slip. ω_1 is the angular velocity of the grid voltage. ω_r is the angular frequency of the rotor. Superscripts $dq+$ and $dq-$ indicate that the vector is measured with respect to the two-phase synchronous reference frames rotating with ω_1 and $-\omega_1$, respectively. Subscripts s and r stand for stator and rotor. Subscripts +, –, and 0 indicate positive-, negative- and zero-sequence components, respectively.

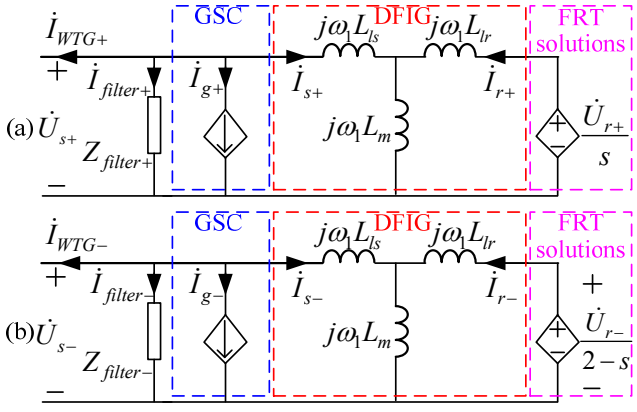

Fig. 2. Equivalent circuits of a DFIG-based WTG represented with phasors: (a) positive-sequence equivalent circuit; (b) negative-sequence equivalent circuit.

The above modeling is represented with space vectors, while the power system fault analysis is built on the phasor notation [37]. Appendix presents the transformation between phasor and space vector notations in the sequence domain. Phasors are represented with dot superscripts in this paper. The above expressions can be transformed into phasors, and the positive- and negative-sequence equivalent circuits of the DFIG-based

WTG can be obtained as in Fig. 2 (a) and Fig. 2 (b).

L_{ls} and L_{lr} are the stator and rotor leakage inductances, namely

$$L_{ls} = L_s - L_m \quad L_{lr} = L_r - L_m \tag{4}$$

According to Fig. 2, the positive- and negative-sequence stator current vectors are expressed as

$$\dot{I}_{s+} = \frac{\dot{U}_{s+}}{j\omega_1 L_s} - \frac{L_m}{L_s}\dot{I}_{r+} \quad \dot{I}_{s-} = \frac{\dot{U}_{s-}}{j\omega_1 L_s} - \frac{L_m}{L_s}\dot{I}_{r-} \tag{5}$$

The impact of FRT solutions on the fault current can be represented with the positive- and negative-sequence rotor currents. This impact will be analyzed in Section III.

The positive- and negative-sequence current phasors of the DFIG-based WTG are

$$\dot{I}_{WTG+} = \boldsymbol{I}_{WTG+}^{dq+} = -\frac{\dot{U}_{s+}}{j\omega_1 L_s} + \frac{L_m}{L_s}\boldsymbol{I}_{r+}^{dq+} - \boldsymbol{I}_{g+}^{dq+} - \dot{I}_{filter+} \tag{6}$$

$$\dot{I}_{WTG-} = (\boldsymbol{I}_{WTG-}^{dq-})^* = -\frac{\dot{U}_{s-}}{j\omega_1 L_s} + \frac{L_m}{L_s}(\boldsymbol{I}_{r-}^{dq-})^* - (\boldsymbol{I}_{g-}^{dq-})^* - \dot{I}_{filter-} \tag{7}$$

where the superscript * stands for the conjugate complex, and

$$\dot{I}_{filter+} = \frac{\dot{U}_{s+}}{Z_{filter+}} \quad \dot{I}_{filter-} = \frac{\dot{U}_{s-}}{Z_{filter-}} \tag{8}$$

where $Z_{filter+}$ and $Z_{filter-}$ are the positive- and negative-sequence impedances of the DFIG filter.

B. Framework of the Proposed Model

The proposed sequence-domain model is built on the framework shown in Fig. 3. Initially, the user should specify the basic configuration of the DFIG-based WTG, including FRT types, parameters, and the grid code requirements. In short circuit computation, the proposed model will receive the positive- and negative-sequence voltage phasors from the iterative solver (as two inputs of the proposed model). Then, the positive- and negative-sequence current phasors contributed by the DFIG-based WTG (as two outputs of the proposed model) are calculated and updated for the next iteration. The detailed computation processes, under different FRT control schemes and protection circuit, are in Section III. Then, the desired current and voltage by the control are calculated in Section IV to determine whether crowbar circuit would be triggered. If so, the current phasors will be corrected according to Section III.E.

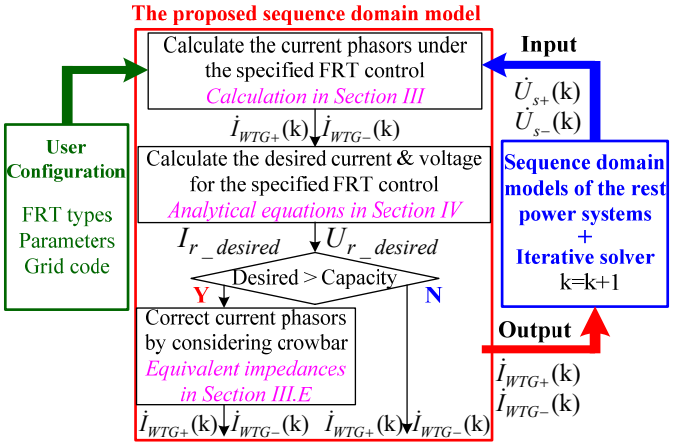

Fig. 3. Framework of the proposed sequence domain model.

III. Current Phasor Calculation for FRT Solutions

This section briefly introduces the typical FRT control schemes and crowbar circuit, and then provides the calculation of current phasors for each FRT configuration.

A. Positive- and Negative-sequence Stator Voltage Reference Frames

As two inputs of the proposed model, the positive- and negative-sequence voltage phasors are

$$\dot{U}_{s+} = U_{s+}e^{j\varphi_+} \quad \dot{U}_{s-} = U_{s-}e^{j\varphi_-} \tag{9}$$

where U_{s+} and U_{s-} are the magnitudes of positive- and negative-sequence voltage phasors, respectively. φ_+ *and* φ_- are the phase angles of the positive- and negative-sequence voltage phasors.

Per Appendix, the corresponding voltage vectors are

$$\boldsymbol{U}_{s+}^{dq+} = \dot{U}_{s+} = U_{s+}e^{j\varphi_+} \quad \boldsymbol{U}_{s-}^{dq-} = (\dot{U}_{s-})^* = U_{s-}e^{-j\varphi_-} \tag{10}$$

The current vectors should be rotated to the positive- and negative-sequence stator voltage reference frames (denoted by superscripts *SVR*+ and *SVR*-) as (11) and (12) so that the real and imaginary parts stand for the active and reactive components, respectively.

$$\boldsymbol{X}_{+}^{SVR+} = \boldsymbol{X}_{+}^{dq+}e^{-j\varphi_+} = X_{d+}^{SVR+} + jX_{q+}^{SVR+} \tag{11}$$

$$\boldsymbol{X}_{-}^{SVR-} = \boldsymbol{X}_{-}^{dq-}e^{j\varphi_-} = X_{d-}^{SVR-} + jX_{q-}^{SVR-} \tag{12}$$

B. Current Phasor Calculation under BPSC

For the BPSC scheme, current references and inner-loop control are all designed for positive-sequence quantities. The calculation procedure is shown in Fig. 4 and detailed below.

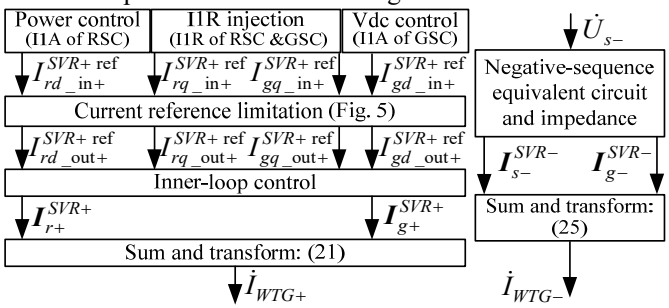

Fig. 4. Calculation procedure of the positive- and negative-sequence current phasors of DFIG-based WTG controlled with BPSC.

(1) Positive-sequence Active Current (I1A) Reference of RSC

For the purpose of short circuit calculation, the output active power reference can be assumed as a given constant P^{ref}. Thus, the required I1A of the WTG is

$$I_{WTGd+}^{SVR+} = \frac{P^{\text{ref}}}{\eta U_{s+}} \tag{13}$$

where the superscript ref stands for the reference. η is the ratio between output active power and electromagnetic power.

The partial active power contributed by stator winding and grid side converter (GSC) is naturally allocated according to the slip [31]. Per (5), the I1A component of stator and rotor current references are

$$I_{sd\_in+}^{SVR+\,ref} = \frac{-1}{1-s}\frac{P^{\text{ref}}}{\eta U_{s+}} \quad I_{rd\_in+}^{SVR+\,ref} = -\frac{L_s}{L_m}I_{sd\_in+}^{SVR+\,ref} \tag{14}$$

where the subscripts in and out stand for the reference before and after the current limiter, respectively.

(2) Positive-sequence Reactive Current (I1R) Reference of RSC

According to the grid code [22], the required I1R can be generally expressed as

$$I_{WTGq+}^{SVR+} = -K_{V+}(1-U_{s+}) \tag{15}$$

where K_{V+} is the slop of the I1R injection requirement.

The required I1R in (15) is mainly contributed by the stator winding and RSC control. By substituting (15) into (1), the I1R component of rotor current reference before the limiter is

$$I_{rq\_in+}^{SVR+\ ref} = -\frac{L_s}{L_m}K_{V+}(1-U_{s+}) - \frac{U_{s+}}{\omega_1 L_m} \tag{16}$$

During FRT, I1R has the priority, and the rest of the current capacity of RSC will be assigned to the I1A component [24]. The limiter and coordination elements are shown in Fig. 5.

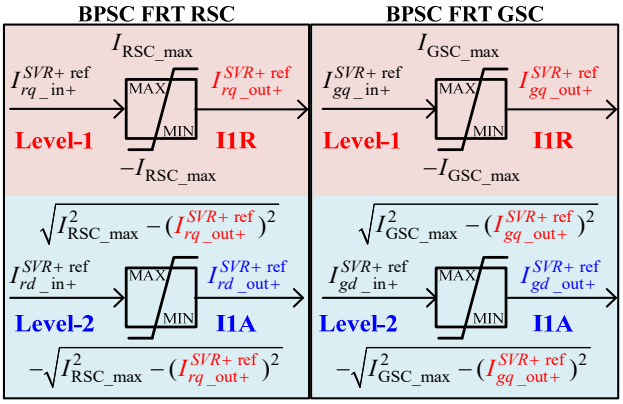

Fig. 5 Current reference limitation and coordination in BPSC.

(3) I1A Reference of GSC

The DC-link voltage control is designed to maintain the DC capacitor voltage. The I1A current component of the GSC can be expressed with GSC active power P_g as

$$I_{gd\_in+}^{SVR+\ ref} = P_g / U_{s+} \tag{17}$$

As a simplification, the active power of GSC can be expressed with that of the rotor winding, namely

$$P_g \approx P_r = \mathrm{Re}[\boldsymbol{U}_{r+}^{SVR+}(\boldsymbol{I}_{r+}^{SVR+})^* + \boldsymbol{U}_{r-}^{SVR-}(\boldsymbol{I}_{r-}^{SVR-})^*] \tag{18}$$

More details on the positive- and negative-sequence rotor voltage vectors will be given in Section IV.

(4) I1R Reference of GSC

If the I1R component of the stator current does not reach the required value in (15), GSC will contribute the rest of the required I1R as

$$I_{gq\_in+}^{SVR+\ ref} = K_{V+}(1-U_{s+}) + \frac{U_{s+}}{\omega_1 L_s} + \frac{L_m}{L_s} I_{rq\_out+}^{PLL+\ ref} \tag{19}$$

(5) Inner-loop Control

With the inner-loop control, the above positive-sequence current references can be quickly realized. However, owing to the sampling filters and PWM modulation, a phase shift represented by an angle β is introduced [38]. According to (11), the positive-sequence rotor and GSC current vectors are

$$\boldsymbol{I}_{r+}^{dq+} = \boldsymbol{I}_{r\_out+}^{SVR+\ ref} e^{j(\varphi_+ + \beta)} \quad \boldsymbol{I}_{g+}^{dq+} = \boldsymbol{I}_{g\_out+}^{SVR+\ ref} e^{j(\varphi_+ + \beta)} \tag{20}$$

Thus, according to (6), the positive-sequence current phasor of the DFIG-based WTG is

$$\dot{I}_{WTG+} = -\frac{\dot{U}_{s+}}{j\omega_1 L_s} + (\frac{L_m}{L_s}\boldsymbol{I}_{r\_out+}^{SVR+\ ref} - \boldsymbol{I}_{g\_out+}^{SVR+\ ref})e^{j(\varphi_+ + \beta)} - \dot{I}_{filter+} \tag{21}$$

(6) Negative-sequence Current Phasor

Although there is no negative-sequence inner-loop controller in the BPSC, negative-sequence rotor current would still generate negative-sequence rotor voltage through the coupled inner-loop control and thus introduces a low-impedance branch in the negative-sequence network [30]. The equivalent stator inductance proposed in [39] can be introduced to calculate the negative-sequence stator current vector by one step, namely

$$\boldsymbol{I}_{s-}^{dq-} = \frac{\boldsymbol{U}_{s-}^{dq-}}{-j\omega_1 \boldsymbol{L}_{eqs.DCS}(-\omega_1)} \tag{22}$$

where

$$\boldsymbol{L}_{eqs.DCS}(-\omega_1) = L_s \frac{K_{pi\_RSC} - j2\omega_1\sigma L_r}{K_{pi\_RSC} - j2\omega_1 L_r} \quad \sigma = 1 - \frac{L_m^2}{L_s L_r} \tag{23}$$

where K_{pi_RSC} is the proportional parameter of the RSC inner-loop controller.

Similarly, the negative-sequence GSC current can be simplified as

$$\boldsymbol{I}_{g-}^{dq-} = \frac{\boldsymbol{U}_{s-}^{dq-}}{K_{pi\_GSC}} \approx 0 \tag{24}$$

where K_{pi_GSC} is the proportional parameter of the GSC inner-loop controller.

Thus, according to (7), the negative-sequence current phasor of the DFIG-based WTG is

$$\dot{I}_{WTG-} = -\frac{\dot{U}_{s-}}{Z_{DFIG.BPSC-}} - \frac{\dot{U}_{s-}}{K_{pi\_GSC}} - \dot{I}_{filter-} \tag{25}$$

Accounting the angle shift and the stator resistance, the negative-sequence equivalent impedance of the DFIG is

$$Z_{DFIG.BPSC-} = (R_s + j\omega_1 L_s \frac{K_{pi\_RSC} + j2\omega_1\sigma L_r}{K_{pi\_RSC} + j2\omega_1 L_r})e^{j\beta} \tag{26}$$

C. Current Phasor Calculation under the PNSC-Tem scheme

In the PNSC-Tem control scheme, the positive- and negative-sequence current components are decomposed using the measurements and then independently controlled with positive- and negative-sequence inner-loop controllers. The calculation procedure of the positive- and negative-sequence current phasors under PNSC-Tem is shown in Fig. 6. The positive-sequence current references and phasor before the current limitation are the same as that of BPSC in Section III.B as they both comply with the same I1R requirement.

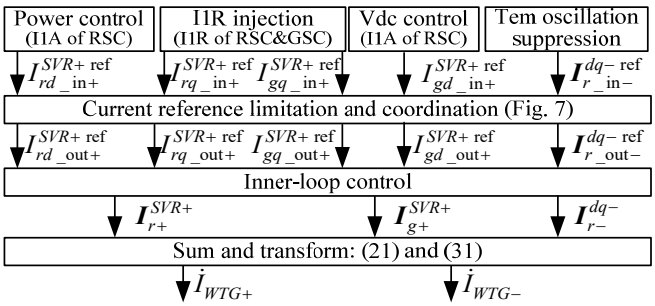

Fig. 6. Calculation procedure of the positive- and negative-sequence current phasors of DFIG-based WTG controlled with PNSC-Tem.

To eliminate the double grid frequency oscillation in Tem, the negative-sequence rotor current references in [26] can be

expressed with space vector as

$$\boldsymbol{I}_{r\_\text{in}-}^{dq-*}=\frac{\boldsymbol{U}_{s-}^{dq-}}{U_{s+}}(\boldsymbol{I}_{r\_\text{out}+}^{SVR+\text{ ref}})^{*} \tag{27}$$

The negative-sequence current references of the GSC can also be designed to suppress the oscillations of DC voltage or to balance the current of the WTG. Since the negative-sequence current of the GSC is much smaller than that of the stator current, it is simplified in the short circuit calculation, as

$$\boldsymbol{I}_{g-}^{dq-\text{ ref}}=0 \tag{28}$$

Per (27), the magnitudes of the positive- and negative-sequence rotor current vectors are

$$\left|\boldsymbol{I}_{r\_\text{in}-}^{dq-\text{ ref}}\right|=(U_{s-}/U_{s+})\left|\boldsymbol{I}_{r\_\text{out}+}^{SVR+\text{ ref}}\right| \tag{29}$$

The current reference limitation is designed in Fig. 7 and

$$p_1=U_{s+}/(U_{s+}+U_{s-}) \tag{30}$$

According to (7), the negative-sequence current phasor of the DFIG-based WTG is

$$\dot{I}_{WTG-}=-\frac{\dot{U}_{s-}}{j\omega_1 L_s}+\frac{L_m}{L_s}(\boldsymbol{I}_{r\_\text{in}-}^{dq-})^{*}e^{-j\beta}-\dot{I}_{filter-} \tag{31}$$

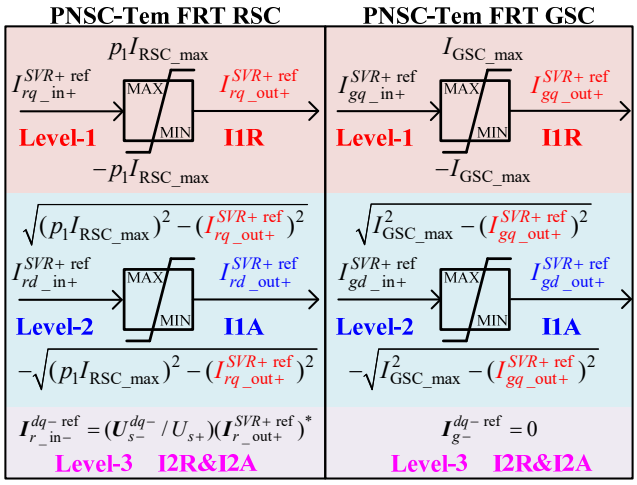

Fig. 7. Current reference limitation and coordination in PNSC-Tem.

D. Current Phasor Calculation under the PNSC-I12R scheme

The calculation process of the positive- and negative-sequence current phasors under PNSC-I12R is shown in Fig. 8, and the limiter and coordination elements are shown in Fig. 9. The positive-sequence current references and phasor before the current limiter are the same as that of BPSC in Section III.B.

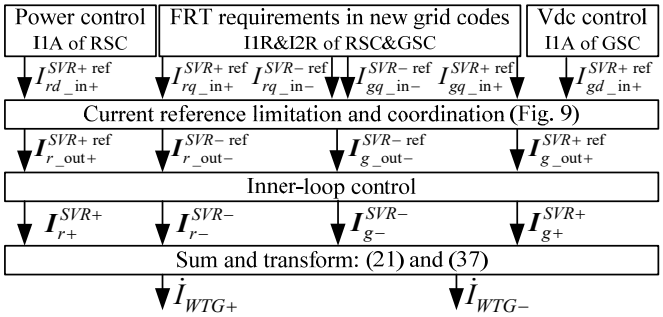

Fig. 8. Processes of calculating the positive- and negative-sequence current phasors of DFIG-based WTG controlled with PNSC-I12R.

The required I2R in grid codes [27]-[29] is expressed with

$$\boldsymbol{I}_{WTG-}^{SVR-}=j\boldsymbol{I}_{WTGq-}^{SVR-}=-jK_{V-}\boldsymbol{U}_{s-} \tag{32}$$

where K_{V-} is the slope of the I2R injection requirement.

In PNSC-I12R, the I2R is also mainly contributed by stator current which enhances the control capability of the RSC during asymmetrical faults [30]. The corresponding rotor current reference is

$$I_{rq\_\text{in}-}^{SVR-\text{ ref}}=\left(\frac{1}{\omega_1 L_m}-\frac{L_s K_{V-}}{L_m}\right)U_{s-} \tag{33}$$

When the rotor current reference exceeds the threshold in Fig. 9, the I2R component in the stator current is

$$I_{sq-}^{SVR-}=-(L_m/L_s)I_{rq\_\text{out}-}^{SVR-\text{ ref}}+U_{s-}/(\omega_1 L_s) \tag{34}$$

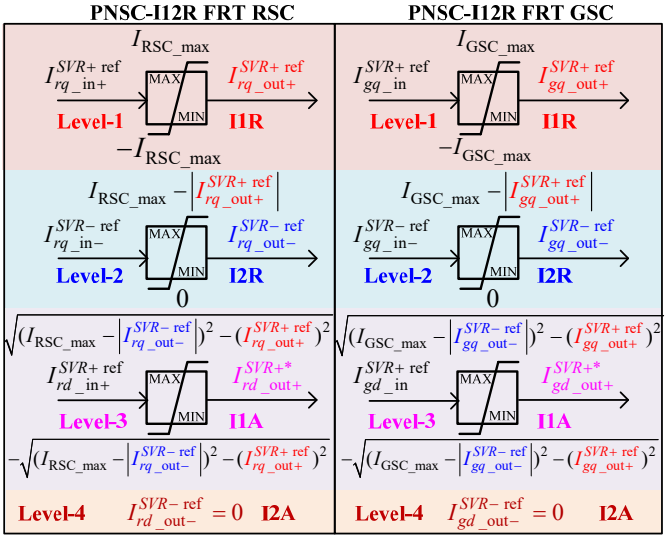

Fig. 9. Current reference limitation and coordination in PNSC-I12R.

The rest of the I2R need to be contributed by the GSC by

$$I_{gq\_\text{in}-}^{SVR-\text{ ref}}=K_{V-}U_{s-}-I_{sq-}^{SVR-}=K_{V-}U_{s-}+\frac{L_m}{L_s}I_{rq\_\text{out}-}^{SVR-\text{ ref}}-\frac{U_{s-}}{\omega_1 L_s} \tag{35}$$

Similarly, the angle shift introduced by the inner-loop control should also be considered. According to (12), the rotor current and GSC current vectors are

$$\boldsymbol{I}_{r-}^{dq-}=jI_{rq\_\text{out}-}^{SVR-\text{ ref}}e^{j(\beta-\varphi_-)}\quad \boldsymbol{I}_{g-}^{dq-}=jI_{gq\_\text{out}-}^{SVR-\text{ ref}}e^{j(\beta-\varphi_-)} \tag{36}$$

Thus, according to (7), the negative-sequence current phasor of the DFIG-based WTG is

$$\dot{I}_{WTG-}=-\frac{\dot{U}_{s-}}{j\omega_1 L_s}-j\left(\frac{L_m}{L_s}I_{rq\_\text{out}-}^{SVR-*}-I_{gq\_\text{out}-}^{SVR-*}\right)e^{j(\varphi_--\beta)}-\dot{I}_{filter-} \tag{37}$$

E. Current Phasor Calculation under Crowbar Protection

During severe voltage dip and unbalance, crowbar protection can operate. The consequent positive- and negative-sequence rotor voltage vectors are

$$\boldsymbol{U}_{r+}^{dq+}=-R_{re}\boldsymbol{I}_{r+}^{dq+}\quad \boldsymbol{U}_{r-}^{dq-}=-R_{re}\boldsymbol{I}_{r-}^{dq-} \tag{38}$$

where $R_{re}=R_r+R_c$. R_c is the per unit crowbar resistance seen from the stator side. For the aggregated model of the WTGs, the equivalent per unit crowbar resistance is

$$R_c(\text{pu})=\frac{R_c(\Omega)}{Z_{base}(\Omega)}\frac{1}{(N_r/N_s)^2}\frac{1}{N_{WTG}} \tag{39}$$

where Z_{base} is the base impedance in per unit system. N_r/N_s is the turns ratio between rotor and stator windings of the DFIG. N_{WTG} is the number of WTGs in the aggregated WP.

The positive- and negative-sequence stator current can also

be calculated with the stator equivalent impedance [40] as

$$\dot{I}_{s+} = \dot{U}_{s+} / Z_{DFIG.\text{Crowbar}+} \quad \dot{I}_{s-} = \dot{U}_{s-} / Z_{DFIG.\text{Crowbar}-} \tag{40}$$

where the positive- and negative-sequence impedances of the DFIG, under crowbar protection, are

$$\begin{aligned} Z_{DFIG.\text{Crowbar}+} &= R_s + j\omega_1 L_s \frac{js\omega_1\sigma L_r + R_{re}}{js\omega_1 L_r + R_{re}} \\ Z_{DFIG.\text{Crowbar}-} &= R_s + j\omega_1 L_s \frac{j(2-s)\omega_1\sigma L_r + R_{re}}{j(2-s)\omega_1 L_r + R_{re}} \end{aligned} \tag{41}$$

During crowbar protection, RSC is blocked and there is no active power that flows into the DC link capacitor through RSC. In this way, GSC can spare almost all its current capacity to provide the required I1R in compensating the I1R absorbed by DFIG during crowbar activation. The GSC current vectors are

$$\boldsymbol{I}_{g+}^{dq+} = jI_{\text{GSC\_max}} \quad \boldsymbol{I}_{g-}^{dq-} \approx 0 \tag{42}$$

Thus, by substituting (40) and (42) into (6) and (7), the positive- and negative-sequence current phasors of the DFIG-based WTG during crowbar protection are

$$\dot{I}_{WTG+} = -\frac{\dot{U}_{s+}}{Z_{DFIG.\text{Crowbar}+}} - \frac{\dot{U}_{s+}}{Z_{filter+}} - jI_{\text{GSC\_max}} \tag{43}$$

$$\dot{I}_{WTG-} = -\frac{\dot{U}_{s-}}{Z_{DFIG.\text{Crowbar}-}} - \frac{\dot{U}_{s-}}{Z_{filter-}} \tag{44}$$

IV. Operating Criterion Of Crowbar Protection

For a certain fault scenario and a given FRT control scheme, it is important to determine if the capacity of converters is sufficient. If the desired voltage or current by the control exceeds the capacity of the RSC, the crowbar must operate. It would significantly change the fault current phasors. In this section, explicit expressions are proposed to derive the operating criterion of the crowbar circuit.

A. Desired Current and RSC Current Capacity

According to (5), the rotor current phasors can be expressed with stator current and voltage phasors by

$$\dot{I}_{r+} = -\frac{L_s}{L_m}\dot{I}_{s+} + \frac{\dot{U}_{s+}}{j\omega_1 L_m} \quad \dot{I}_{r-} = -\frac{L_s}{L_m}\dot{I}_{s-} + \frac{\dot{U}_{s-}}{j\omega_1 L_m} \tag{45}$$

Since the positive-sequence phasor rotates with $s\omega_1$ while the negative-sequence phasor rotates with $(2\text{-}s)\omega_1$ with respect to the rotor winding, the maximum possible rotor current in a phase can be assessed as follows

$$I_{r\_desired} = \left|\dot{I}_{r+}\right| + \left|\dot{I}_{r-}\right| \tag{46}$$

In terms of the current capacity, the RSC of DFIG-based WTGs can typically withstand up to 200% of its rated current for a very short period of time, and only about 120% of its rated current for the fundamental components during FRT [41]. So the current criteria for crowbar operation is

$$I_{r\_desired} > I_{\text{RSC\_max}} \tag{47}$$

where $I_{\text{RSC\_max}}$ is the maximum rotor current capacity specified by the manufactures.

B. Desired Voltage and RSC Voltage Capacity

According to (1) and (2), the positive- and negative-sequence rotor voltage vectors are expressed with rotor current and stator voltage vectors by

$$\boldsymbol{U}_{r+}^{SVR+} \cong s(j\omega_1\sigma L_r \boldsymbol{I}_{r+}^{SVR+} + \frac{L_m}{L_s}U_{s+}) \tag{48}$$

$$\boldsymbol{U}_{r-}^{SVR-} \cong (2-s)(-j\omega_1\sigma L_r \boldsymbol{I}_{r-}^{SVR-} + \frac{L_m}{L_s}U_{s-}) \tag{49}$$

The RSC desired rotor voltage by the control is calculated as

$$U_{r\_desired} = \left|\boldsymbol{U}_{r+}^{SVR+}\right| + \left|\boldsymbol{U}_{r-}^{SVR-}\right| \tag{50}$$

The maximum output voltage of the RSC is determined by the rated DC link voltage (U_{dc}^{ref}) and the modulation scheme. Considering 2-level voltage source converter (VSC) topology and space vector modulation (SVM), the voltage criterion for crowbar activation is given as follows

$$U_{r\_desired} > \frac{4}{\pi}\frac{U_{dc}^{\text{ref}}}{U_{base}\sqrt{3}}\frac{1}{N_r / N_s} \tag{51}$$

where U_{base} is the base stator voltage in per unit system. $4/\pi$ considers the maximum magnitude of the fundamental component under severe over-modulation [19]. If the RSC is made of other matrix or multilevel converter topologies [42]-[43], the right hand side of (51) should be adjusted accordingly.

V. Demonstration

This section verifies the proposed sequence model by comparing the results of the steady state iterative solution and EMT simulations for the EPRI benchmark system. The phasor characteristics of the DFIG are presented, and the efficiency and limitations of the proposed model are discussed.

A. Test System and Scenarios

The EPRI benchmark system shown in Fig. 10 is studied in this paper using the proposed steady state modeling approach and EMT simulations. In the studied system, 45×1.5MW DFIG-based WTGs are aggregated to form the WP for studying faults on the system side. The WP is connected to a 120 kV transmission network through BUS1. All results presented in this section are in per-unit referring to the apparent power of the WP (75MVA). Before the fault inception, all WTGs are operating in super-synchronous state (s=-0.2).

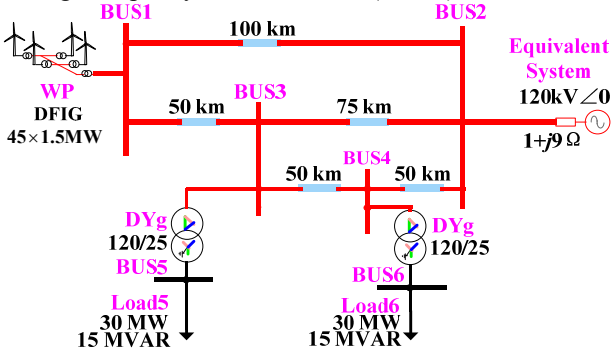

Fig. 10. 120kV 60Hz EPRI benchmark system.

The detailed parameters of the DFIG-based WTGs and 120kV transmission lines are listed in Table I and Table II, respectively. More details on the EPRI benchmark system are available in [21].

It is also available in EMTP software [34] as an example. The proposed model is validated with an extensive set of scenarios totaling 216 cases by considering 3 control types (BPSC/PNSC-Tem/PNSC-I12R), 6 fault locations (BUS1-BUS6), 4 fault types (three-phase/single-phase/double-line-to-ground/line-to-line short circuits), and 3 fault resistances (0/1/10 Ohm). Due to the page limit, only a demonstrative set of results is presented.

TABLE I PARAMETERS OF 1.5MW DFIG-BASED WTG

Parameter	Value	Parameter	Value
U_{base}	469.485 V	$I_{\text{RSC max}}$	1.200 pu
P_N	1.5 MW	$I_{\text{GSC max}}$	0.360 pu
S_{base}	1.667 MVA	$K_{pi\ \text{RSC}}$	0.820
R_s	0.033 pu	$K_{ii\ \text{RSC}}$	12.13
R_r	0.026 pu	$K_{pi\ \text{GSC}}$	5
R_c	0.14 pu (0.25Ω)	$K_{ii\ \text{GSC}}$	98
ω_1	120π rad/s	K_{V+}	2
$\omega_1 L_s$	3.08 pu	K_{V-}	2
$\omega_1 L_r$	3.06 pu	K_{pPLL}	180
$\omega_1 L_m$	2.90 pu	K_{iPLL}	1000
U_{dc}^{ref}	1150 V	N_r/N_s	3:1
η	96.60%	β	-1.09°
$Z_{filter+}$=$Z_{filter-}$= 0.0005-11.1167 pu			

TABLE II 120 kV TRANSMISSION LINE PARAMETERS

	Positive/negative-sequence	Zero-sequence
Resistance	0.1270 Ω/km	0.3125 Ω/km
Inductance	0.4794 Ω/km	1.6621 Ω/km
Capacitance	3.4788 μS/km	1.8166 μS/km

B. Accuracy and Phasor Characteristics

In each EMT simulation, short circuit is applied at 2s and is removed at 3s to clearly observe the steady state periods. Three-phase time-domain instantaneous values are converted into phasors using the built-in extraction components in EMT software. As an example, Fig. 11 demonstrates three-phase unbalanced voltage and extracted phasor components at the WTG terminal under a bolted phase-A to phase-B to ground (ABG) fault at BUS3.

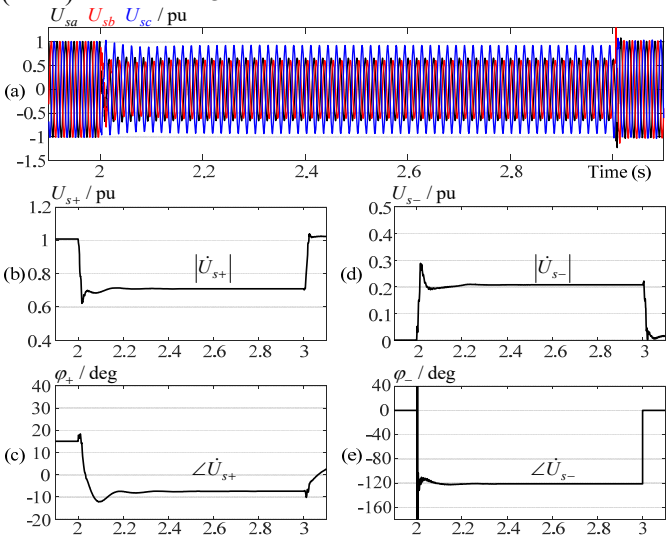

Fig. 11. Three-phase voltage obtained by EMT simulation and the extracted positive- and negative-sequence phasors under a bolted ABG short circuit at BUS3 (a) three-phase stator voltage (b) positive-sequence voltage magnitude (c) positive-sequence voltage angle (d) negative-sequence voltage magnitude (e) negative -sequence voltage angle (WTG is controlled with PNSC-I12R)

As shown in Fig. 11 (c), the measured phasors reach to the final steady state after oscillating around it for about 100ms. This transient is related to the response of the phase-lock loop (PLL) and may have an impact on fast time domain protection elements. However, the focus of this paper is the steady-state component of the short circuit current.

By using the proposed sequence-domain model and the MANA-based iterative steady state short circuit solver [35], the positive- and negative-sequence voltage and current phasors obtained in different fault scenarios are tabulated in Table III to Table VII. The control types and fault resistances are indicated in parenthesis. Based on the results, the relative error of an iterative solution, with respect to its EMT simulation counterpart, is calculated as follows

$$\text{relative error} = \left|\dot{X}_{\text{iteration}} - \dot{X}_{\text{EMT}}\right| / \left|\dot{X}_{\text{EMT}}\right| \% \qquad (52)$$

where $\dot{X}$ stands for a voltage or current phasor. If the subscript is iteration, this means that the phasor is obtained by an iterative solution in steady state whereas EMT indicates a phasor obtained by extraction from detailed time domain simulations.

Table III shows the results for bolted symmetrical faults at different buses considering the BPSC scheme. For varying fault resistances, similar accuracies are observed, i.e., the relative error is less than 3.5%. When the fault gets closer to the WP, the voltage dip is more significant and the current phasor lags voltage phasor by 90° and the WP mainly provides I1R as described in (15). When the fault is electrically distant from the WP (for example at BUS5 or BUS6), the voltage dip is weak and the angle difference between voltage and current phasors is small. The WP mainly provides I1A as in normal operation conditions. For symmetrical fault scenarios, the WP provides only positive sequence current and has the same response with different control schemes (BPSC/PNSC-Tem/PNSC-I12R).

Under a bolted three-phase (ABC) fault at BUS1 or BUS2, the WP is disconnected from the rest of the network and loses synchronism. The PLL frequency starts deviating from the grid frequency [44] as shown in Fig. 12 (a). As a result, the phase angles of the voltage and current phasors obtained by EMT simulations will not reach steady state as shown in Fig. 12 (b) to (e). In these cases, the iterative solver switches the WP to island mode. Note that, the proposed model is intended to be used for short circuit computations on the system side and not within the WP. Islanded mode of operation with grid forming control capabilities is not considered in this work.

TABLE III PHASORS FOR ABC SHORT CIRCUITS (BPSC, 0 OHM)

Fault bus	Phasors	EMTP	Iterative solution	Error
BUS3	$\dot{U}_{s+}$	$0.497\angle -18.8^\circ$	$0.501\angle -18.7^\circ$	0.8438%
	$\dot{I}_{WTG+}$	$1.053\angle -112.9^\circ$	$1.045\angle -112.8^\circ$	0.7323%
BUS4	$\dot{U}_{s+}$	$0.656\angle 23.8^\circ$	$0.663\angle 23.6^\circ$	1.0264%
	$\dot{I}_{WTG+}$	$1.069\angle -20.9^\circ$	$1.073\angle -19.9^\circ$	1.8081%
BUS5	$\dot{U}_{s+}$	$0.830\angle 28.8^\circ$	$0.844\angle 27.3^\circ$	3.1405%
	$\dot{I}_{WTG+}$	$1.164\angle 7.4^\circ$	$1.136\angle 7.0^\circ$	2.5657%
BUS6	$\dot{U}_{s+}$	$0.885\angle 23.8^\circ$	$0.900\angle 22.7^\circ$	2.5918%
	$\dot{I}_{WTG+}$	$1.046\angle 6.7^\circ$	$1.046\angle 6.7^\circ$	1.8903%

For a phase-A to ground (AG) fault at BUS1-BUS3, the BPSC controlled DFIG activates its crowbar protection. This is because the rotor current exceeds the capacity as shown with (47). In these scenarios, the angle differences between voltage

and current phasors are all less than 12°. Because, in terms of I1A, the slip is still negative and the DFIG acts like a significant negative resistance. In terms of I1R, the GSC partially compensates I1R absorbed by the DFIG as shown in (19).

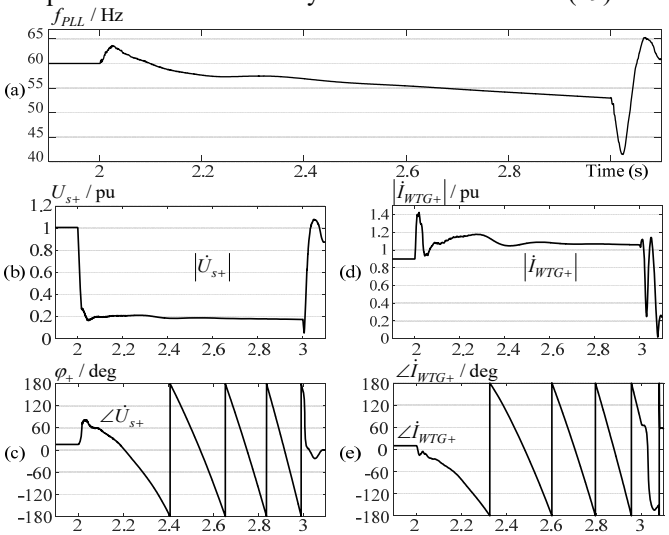

Fig. 12. PLL frequency and positive-sequence phasors as simulated in EMT for a bolted ABC short circuit at BUS1 (a) PLL frequency (b) positive-sequence voltage magnitude (c) positive-sequence voltage angle (d) positive-sequence current magnitude (e) positive-sequence current angle (WTG is controlled with PNSC-I12R)

TABLE IV PHASORS FOR AG SHORT CIRCUITS (BPSC, 10 OHM)

Fault bus	Phasors	EMTP	Iterative solution	Error
BUS1 (Crowbar)	$\dot{U}_{s+}$	$0.634\angle 2.9^\circ$	$0.649\angle 2.7^\circ$	2.2942%
	$\dot{I}_{WTG+}$	$0.594\angle 7.7^\circ$	$0.609\angle 8.1^\circ$	2.5669%
	$\dot{U}_{s-}$	$0.187\angle -165.2^\circ$	$0.191\angle -165.3^\circ$	2.2349%
	$\dot{I}_{WTG-}$	$0.516\angle -57.5^\circ$	$0.531\angle -58.0^\circ$	2.9556%
BUS2 (Crowbar)	$\dot{U}_{s+}$	$0.795\angle 8.9^\circ$	$0.814\angle 8.6^\circ$	2.3471%
	$\dot{I}_{WTG+}$	$0.758\angle 20.5^\circ$	$0.778\angle 20.8^\circ$	2.6487%
	$\dot{U}_{s-}$	$0.082\angle -153.0^\circ$	$0.083\angle -153.2^\circ$	2.0250%
	$\dot{I}_{WTG-}$	$0.226\angle -45.2^\circ$	$0.234\angle -45.7^\circ$	3.2671%
BUS3 (Crowbar)	$\dot{U}_{s+}$	$0.769\angle 11.8^\circ$	$0.787\angle 11.5^\circ$	2.3391%
	$\dot{I}_{WTG+}$	$0.731\angle 22.5^\circ$	$0.750\angle 22.8^\circ$	2.6392%
	$\dot{U}_{s-}$	$0.085\angle -171.2^\circ$	$0.087\angle -171.4^\circ$	2.4376%
	$\dot{I}_{WTG-}$	$0.235\angle -63.4^\circ$	$0.242\angle -63.9^\circ$	2.8114%
BUS4	$\dot{U}_{s+}$	$0.942\angle 16.6^\circ$	$0.956\angle 16.0^\circ$	1.8211%
	$\dot{I}_{WTG+}$	$0.979\angle 4.3^\circ$	$0.982\angle 5.4^\circ$	2.0131%
	$\dot{U}_{s-}$	$0.066\angle 172.5^\circ$	$0.069\angle 173.2^\circ$	4.3247%
	$\dot{I}_{WTG-}$	$0.136\angle -43.4^\circ$	$0.133\angle -43.6^\circ$	2.2760%
BUS5	$\dot{U}_{s+}$	$1.000\angle 14.3^\circ$	$1.016\angle 13.6^\circ$	1.9993%
	$\dot{I}_{WTG+}$	$0.906\angle 8.1^\circ$	$0.902\angle 9.5^\circ$	2.3339%
	$\dot{U}_{s-}$	$0.014\angle -84.7^\circ$	$0.015\angle -84.7^\circ$	4.8581%
	$\dot{I}_{WTG-}$	$0.029\angle 58.9^\circ$	$0.029\angle 58.5^\circ$	2.3719%
BUS6	$\dot{U}_{s+}$	$1.002\angle 14.5^\circ$	$1.018\angle 13.8^\circ$	2.0072%
	$\dot{I}_{WTG+}$	$0.904\angle 8.6^\circ$	$0.900\angle 9.9^\circ$	2.3454%
	$\dot{U}_{s-}$	$0.010\angle -85.5^\circ$	$0.011\angle -85.7^\circ$	4.7003%
	$\dot{I}_{WTG-}$	$0.021\angle 57.9^\circ$	$0.020\angle 57.5^\circ$	2.3706%

For the rest of AG faults at BUS4 to BUS6, the resulting positive-sequence voltage dip and the rise in negative-sequence voltage are insignificant. Thus, the WTG provides I1R as requested by (15) and then increases its I1A to realize its active power reference. Since BPSC is not equipped with a negative-sequence control scheme, the negative-sequence current output from the DFIG-based WTG is still significant as discussed in [30]. The relative errors in Table IV are typically less than 3.5%, but the maximum relative error can be as high as 5%. It is because the denominator of (52), i.e., the magnitude of the negative-sequence phasor, is very small. In these cases, the maximum error in magnitude and angle are only 0.002 pu and 1°, which are acceptable for protection studies.

TABLE V PHASORS FOR AG SHORT CIRCUITS (PNSC-Tem, 10 Ohm)

Fault bus	Phasors	EMTP	Iterative solution	Error
BUS4	$\dot{U}_{s+}$	$0.942\angle 16.5^\circ$	$0.959\angle 15.2^\circ$	2.9499%
	$\dot{I}_{WTG+}$	$0.979\angle 4.2^\circ$	$0.940\angle 4.3^\circ$	3.9563%
	$\dot{U}_{s-}$	$0.112\angle -150.2^\circ$	$0.114\angle -151.7^\circ$	3.2488%
	$\dot{I}_{WTG-}$	$0.104\angle -162.0^\circ$	$0.100\angle -161.8^\circ$	3.4811%
BUS5	$\dot{U}_{s+}$	$0.999\angle 14.1^\circ$	$1.016\angle 13.6^\circ$	1.9204%
	$\dot{I}_{WTG+}$	$0.906\angle 7.9^\circ$	$0.901\angle 9.4^\circ$	2.7014%
	$\dot{U}_{s-}$	$0.024\angle -50.0^\circ$	$0.024\angle -51.3^\circ$	2.6330%
	$\dot{I}_{WTG-}$	$0.018\angle -55.0^\circ$	$0.018\angle -54.0^\circ$	2.3011%
BUS6	$\dot{U}_{s+}$	$1.001\angle 14.4^\circ$	$1.018\angle 13.8^\circ$	1.9117%
	$\dot{I}_{WTG+}$	$0.904\angle 8.4^\circ$	$0.899\angle 9.9^\circ$	2.7253%
	$\dot{U}_{s-}$	$0.017\angle -50.7^\circ$	$0.017\angle -52.4^\circ$	3.0111%
	$\dot{I}_{WTG-}$	$0.013\angle -55.5^\circ$	$0.013\angle -54.7^\circ$	2.1082%

TABLE VI PHASORS FOR AG SHORT CIRCUITS (PNSC-I12R, 0 Ohm)

Fault bus	Phasors	EMTP	Iterative solution	Error
BUS1	$\dot{U}_{s+}$	$0.737\angle -4.4^\circ$	$0.747\angle -4.4^\circ$	1.3085%
	$\dot{I}_{WTG+}$	$0.595\angle -99.7^\circ$	$0.575\angle -99.8^\circ$	3.4803%
	$\dot{U}_{s-}$	$0.269\angle 174.1^\circ$	$0.274\angle 174.0^\circ$	1.7469%
	$\dot{I}_{WTG-}$	$0.509\angle -94.6^\circ$	$0.524\angle -94.8^\circ$	2.8690%
BUS2	$\dot{U}_{s+}$	$0.876\angle 17.9^\circ$	$0.888\angle 17.4^\circ$	1.5927%
	$\dot{I}_{WTG+}$	$0.915\angle -3.5^\circ$	$0.917\angle -2.3^\circ$	2.1689%
	$\dot{U}_{s-}$	$0.128\angle -179.1^\circ$	$0.132\angle -179.3^\circ$	2.5875%
	$\dot{I}_{WTG-}$	$0.245\angle -87.5^\circ$	$0.252\angle -88.0^\circ$	2.5782%
BUS3	$\dot{U}_{s+}$	$0.888\angle 18.6^\circ$	$0.901\angle 18.2^\circ$	1.6287%
	$\dot{I}_{WTG+}$	$0.956\angle -0.3^\circ$	$0.960\angle 0.9^\circ$	2.1879%
	$\dot{U}_{s-}$	$0.114\angle -178.4^\circ$	$0.117\angle -178.7^\circ$	2.3704%
	$\dot{I}_{WTG-}$	$0.218\angle -86.8^\circ$	$0.224\angle -87.3^\circ$	2.5350%
BUS4	$\dot{U}_{s+}$	$0.934\angle 18.7^\circ$	$0.948\angle 17.7^\circ$	2.2759%
	$\dot{I}_{WTG+}$	$0.990\angle 5.6^\circ$	$0.976\angle 6.3^\circ$	1.8274%
	$\dot{U}_{s-}$	$0.068\angle -179.3^\circ$	$0.070\angle -179.7^\circ$	2.5991%
	$\dot{I}_{WTG-}$	$0.131\angle -87.7^\circ$	$0.134\angle -88.1^\circ$	2.6289%
BUS5	$\dot{U}_{s+}$	$0.944\angle 19.2^\circ$	$0.959\angle 18.3^\circ$	2.2255%
	$\dot{I}_{WTG+}$	$0.975\angle 7.2^\circ$	$0.963\angle 7.9^\circ$	1.8665%
	$\dot{U}_{s-}$	$0.060\angle -129.1^\circ$	$0.061\angle -129.6^\circ$	2.5532%
	$\dot{I}_{WTG-}$	$0.114\angle -37.5^\circ$	$0.117\angle -38.0^\circ$	2.5984%
BUS6	$\dot{U}_{s+}$	$0.963\angle 18.0^\circ$	$0.979\angle 17.1^\circ$	2.1277%
	$\dot{I}_{WTG+}$	$0.950\angle 7.8^\circ$	$0.940\angle 8.8^\circ$	1.9422%
	$\dot{U}_{s-}$	$0.042\angle -130.2^\circ$	$0.043\angle -130.7^\circ$	2.6320%
	$\dot{I}_{WTG-}$	$0.080\angle -38.7^\circ$	$0.082\angle -39.0^\circ$	2.4954%

Under the PNSC-Tem scheme, the crowbar protection is still activated for an AG short circuit at BUS1-BUS3. This is because the desired rotor voltage exceeds the capacity as discussed in (51). The resulting voltage and current phasors in

these cases are identical to those shown in Table IV. Therefore, only the phasors for faults at BUS4 to BUS6 are presented in Table V. Since the negative-sequence current references are accurately estimated by the proposed equations in Section III.C, the relative errors are all within 4%. It is noted that the angle difference between the negative-sequence voltage and current are different from that of Table IV. This is because the PNSC-Tem scheme adjusts the negative sequence current to eliminate the double frequency oscillations.

Under the PNSC-I12R scheme, the crowbar protection does not operate for AG faults at all locations, even under a bolted AG short circuit at BUS1. Because the PNSC-I12R coordinates the rotor current and therefore decreases the desired rotor voltage [30]. As shown in Table VI, the negative-sequence current phasor leads the negative-sequence voltage phasor by 90° to provide the required I2R in (15). For the bolted AG short circuit at BUS1, the positive-sequence current phasor lags the positive-sequence voltage phasor by about 94° to provide the required I1R leading I1A. All the relative errors in Table VI are within 3.5%.

TABLE VII PHASORS FOR ABG SHORT CIRCUITS (PNSC-I12R, 0 Ohm)

Fault bus	Phasors	EMTP	Iterative solution	Error
BUS1 (Crowbar)	$\dot{U}_{s+}$	$0.284\angle 15.1^\circ$	$0.290\angle 14.8^\circ$	2.1560%
	$\dot{I}_{WTG+}$	$0.317\angle -18.8^\circ$	$0.322\angle -17.8^\circ$	2.2280%
	$\dot{U}_{s-}$	$0.167\angle -120.3^\circ$	$0.171\angle -120.5^\circ$	2.7812%
	$\dot{I}_{WTG-}$	$0.464\angle -12.9^\circ$	$0.476\angle -13.2^\circ$	2.5652%
BUS2	$\dot{U}_{s+}$	$0.646\angle -11.2^\circ$	$0.653\angle -11.0^\circ$	1.2003%
	$\dot{I}_{WTG+}$	$0.769\angle -105.6^\circ$	$0.755\angle -105.0^\circ$	2.1008%
	$\dot{U}_{s-}$	$0.262\angle -120.9^\circ$	$0.268\angle -121.1^\circ$	2.1934%
	$\dot{I}_{WTG-}$	$0.496\angle -30.1^\circ$	$0.512\angle -30.3^\circ$	3.1132%
BUS3	$\dot{U}_{s+}$	$0.709\angle -7.4^\circ$	$0.718\angle -7.4^\circ$	1.2075%
	$\dot{I}_{WTG+}$	$0.648\angle -102.1^\circ$	$0.630\angle -102.2^\circ$	2.8327%
	$\dot{U}_{s-}$	$0.208\angle -121.3^\circ$	$0.212\angle -121.5^\circ$	1.9491%
	$\dot{I}_{WTG-}$	$0.393\angle -29.7^\circ$	$0.405\angle -30.0^\circ$	3.0863%
BUS4	$\dot{U}_{s+}$	$0.813\angle 14.8^\circ$	$0.824\angle 14.6^\circ$	1.3720%
	$\dot{I}_{WTG+}$	$0.827\angle -18.3^\circ$	$0.828\angle -16.8^\circ$	2.5933%
	$\dot{U}_{s-}$	$0.146\angle -116.3^\circ$	$0.150\angle -116.6^\circ$	2.4471%
	$\dot{I}_{WTG-}$	$0.279\angle -24.7^\circ$	$0.286\angle -25.1^\circ$	2.5347%
BUS5	$\dot{U}_{s+}$	$0.884\angle 23.9^\circ$	$0.899\angle 22.7^\circ$	2.6072%
	$\dot{I}_{WTG+}$	$1.068\angle 6.5^\circ$	$1.047\angle 6.7^\circ$	1.9729%
	$\dot{U}_{s-}$	$0.046\angle -64.3^\circ$	$0.047\angle -65.0^\circ$	3.1495%
	$\dot{I}_{WTG-}$	$0.088\angle 27.3^\circ$	$0.090\angle 26.6^\circ$	2.7542%
BUS6	$\dot{U}_{s+}$	$0.922\angle 21.0^\circ$	$0.937\angle 20.0^\circ$	2.3142%
	$\dot{I}_{WTG+}$	$1.007\angle 6.8^\circ$	$0.993\angle 7.4^\circ$	1.7577%
	$\dot{U}_{s-}$	$0.032\angle -65.7^\circ$	$0.033\angle -66.2^\circ$	2.8742%
	$\dot{I}_{WTG-}$	$0.062\angle 25.9^\circ$	$0.063\angle 25.3^\circ$	2.5987%

Both the EMT simulations and the iterations show that phase-A to phase-B to ground (ABG) and phase-A to phase-B (AB) faults are more stringent for the DFIG than single-phase-to-ground faults. The resulting negative-sequence voltage magnitude at the WTG terminals is higher. Under BPSC and PNSC-Tem, the crowbar protection is activated, even for an ABG or AB fault at BUS4 with a 10 Ohm fault resistance. The results are not presented due to space constraints. All relative errors are less than 3.5%.

Under PNSC-I12R scheme, the crowbar protection is only activated for a bolted ABG or AB fault at BUS1. The results for ABG short circuits are presented in Table VII. All the relative errors are less than 3.5%.

The proposed steady state model can correctly estimate the operation of crowbar and accurately represent the DFIG-based WTG in the positive- and negative-sequence networks. The relative error is typically within 3.5%, and the absolute errors in magnitude and phase angle are within 0.02pu and 2°, respectively. These errors are due to the predefined tolerance for convergence and mainly because of the simplifications in resistances, power calculations, rotor speed dynamics, and the response of outer-loop controllers.

C. *Efficiency*

The proposed model is integrated into an iterative solver coded in MATLAB. EMT simulations are run in EMTP software. The simulation time in EMTP is set to 3.5 seconds. Time domain solution is obtained using the trapezoidal and backward Euler solvers with a fixed time-step of 50μs. Table VIII shows the execution times for four scenarios. As expected, the proposed solution is much faster since it is in steady state and requires much less computations.

TABLE VIII FAULT SCENARIOS AND EXECUTION TIME

No.	Control type	Short circuit	Execution time	
			EMTP	Iterative
1	BPSC	ABC at BUS4 (10 Ohm)	138.732s	0.113s
2	BPSC (crowbar)	AG at BUS1 (1 Ohm)	139.789s	0.129s
3	PNSC-Tem	ABG at BUS6 (0 Ohm)	130.840s	0.131s
4	PNSC-I12R	AB at BUS3 (0 Ohm)	104.148s	0.129s

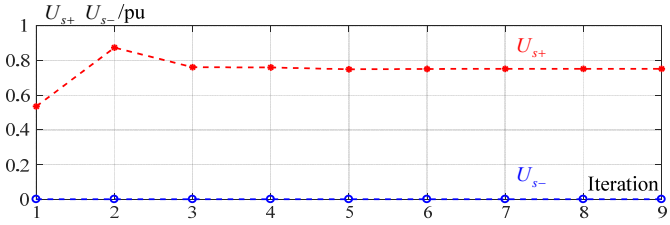

Fig. 13. Positive- and negative-sequence voltage magnitudes at WTG terminal in each iteration for scenario-1 in Table VIII (finished with 9 iterations).

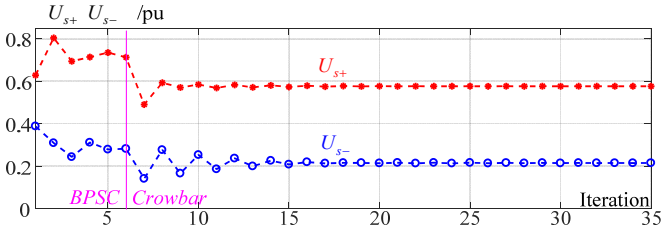

Fig. 14. Positive- and negative-sequence voltage magnitudes at WTG terminal in each iteration for scenario-2 in Table VIII (finished with 35 iterations).

With the proposed model, the iterative solution successfully converges in 212 cases and reports islanded conditions for the remaining 4 cases. The convergence characteristics of the iterative solver can be evaluated by displaying the positive- and negative-sequence voltage magnitudes at the WTG terminal per iteration. Considering a tolerance of 0.0005pu, the convergence characteristics of the selected scenarios in Table VIII are shown in Fig. 13 to Fig. 16. Given the fixed-point nature of the solution approach, the number of iterations can be high, but the advantage is that the main system of equations is factorized for

only once at the first iteration, and the solution time per iteration is insignificant even for networks with thousands of nodes.

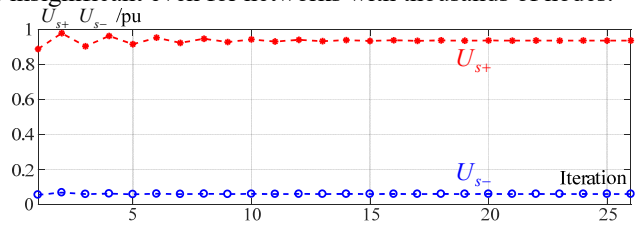

Fig. 15. Positive- and negative-sequence voltage magnitudes at WTG terminal in each iteration for scenario-3 in Table VIII (finished with 26 iterations).

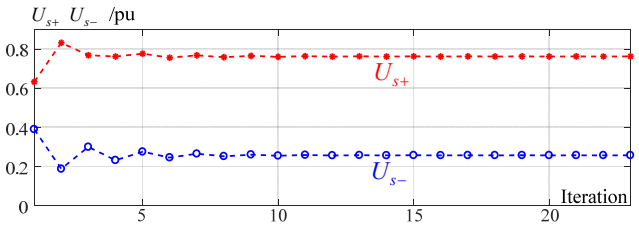

Fig. 16. Positive- and negative-sequence voltage magnitudes at WTG terminal in each iteration for scenario-4 in Table VIII (finished with 23 iterations).

VI. Conclusion

In order to comply with different grid codes, the DFIG-based WTG is configured with various FRT control and protection strategies. This brings complexity and technical challenges for short circuit modeling and analysis. This paper proposes a generic model of the DFIG-based WTG in sequence domain that accounts for three types of typical FRT configurations and the control capacity of converters. When compared with the existing models, the proposed model is an accurate and efficient choice for steady-state short circuit applications considering various grid code requirements and fault scenarios.

The following conclusions can be drawn, viz.,

(1) To comply with FRT requirements in different grid codes, the existing FRT control schemes of the DFIG-based WTG can be generally classified into three types. In earlier grid codes, only positive-sequence reactive current (I1R) was required so the BPSC control scheme has been widely applied. Then, to decrease the mechanical stress of WTG under voltage unbalance, PNSC-Tem has been proposed and adopted by many manufacturers. Recently, some new grid codes introduce additional requirements on the negative-sequence reactive current (I2R). The corresponding control scheme has been denoted by PNSC-I12R in this paper. The proposed model integrates the impacts of these three typical control strategies into a common modeling framework.

(2) For certain fault scenarios, different FRT control schemes correspond to different RSC voltage and current. Since the converters of DFIG-based WTGs are rated with slip power, the desired voltage and current by the control could exceed the capacity of the converters, especially under severe voltage dip or unbalance. In these severe fault scenarios, the FRT control scheme has to be interrupted to trigger the crowbar circuit. As a result, the current phasors of the DFIG-based WTG are significantly changed from that under FRT control. In this proposed model, this characteristic is accounted by estimating the control desired voltage and current by using the proposed explicit equations. By comparing the desired voltage and current with the voltage and current capacity of the RSC, whether the crowbar will operate is determined, and the current phasors are corrected accordingly.

(3) The proposed model is designed to be incorporated into steady state iterative short circuit solvers. It receives positive- and negative-sequence voltage phasors from the main iterative solver, and then updates the positive- and negative-sequence current phasors with the procedure shown in Fig. 3.

(4) The proposed model is validated by comparisons with detailed EMT simulations using the EPRI benchmark system in 216 scenarios. The results show that, compared with the EMT-type model, the proposed model is accurate and has much less execution time in calculating the voltage and current phasors considering different fault locations, fault types and fault resistances.

Considering the improved integrity of the proposed model with respect to the existing phasor models and its efficiency, the future applications include

(1) Batch protection studies considering various fault scenarios in terms of different short circuit types and locations.

(2) Investigating the impact of FRT configurations of the DFIG-based WTGs on power system protection elements.

(3) Examining the settings of protective relays in wind power integration scenarios.

Appendix

A set of three-phase asymmetrical quantities are

$$\begin{aligned} x_a &= X_a \cos(\omega_1 t + \theta_a) \\ x_b &= X_b \cos(\omega_1 t + \theta_b) \\ x_c &= X_c \cos(\omega_1 t + \theta_c) \end{aligned} \tag{53}$$

The positive-, negative- and zero-sequence phasors are

$$\begin{bmatrix} \dot{X}_+ \\ \dot{X}_- \\ \dot{X}_0 \end{bmatrix} = \begin{bmatrix} X_+ e^{j\theta_+} \\ X_- e^{j\theta_-} \\ X_0 e^{j\theta_0} \end{bmatrix} = \frac{1}{3}\begin{bmatrix} 1 & e^{j(2\pi/3)} & e^{-j(2\pi/3)} \\ 1 & e^{-j(2\pi/3)} & e^{j(2\pi/3)} \\ 1 & 1 & 1 \end{bmatrix} \begin{bmatrix} X_a e^{j\theta_a} \\ X_b e^{j\theta_b} \\ X_c e^{j\theta_c} \end{bmatrix} \tag{54}$$

The positive- and negative-sequence space vectors are

$$\boldsymbol{X}^{\alpha\beta} = x_\alpha + j\, x_\beta = \boldsymbol{X}_+^{\alpha\beta} + \boldsymbol{X}_-^{\alpha\beta} \tag{55}$$

where

$$\begin{bmatrix} x_\alpha \\ x_\beta \end{bmatrix} = \frac{2}{3}\begin{bmatrix} 1 & -1/2 & -1/2 \\ 0 & \sqrt{3}/2 & -\sqrt{3}/2 \end{bmatrix} \cdot \begin{bmatrix} x_a \\ x_b \\ x_c \end{bmatrix} \tag{56}$$

$$\boldsymbol{X}_+^{\alpha\beta} = \boldsymbol{X}_+^{dq+} e^{j\omega_1 t} \quad \boldsymbol{X}_+^{dq+} = X_+ e^{j\theta_+} \tag{57}$$

$$\boldsymbol{X}_-^{\alpha\beta} = \boldsymbol{X}_-^{dq-} e^{-j\omega_1 t} \quad \boldsymbol{X}_-^{dq-} = X_- e^{-j\theta_-} \tag{58}$$

The transformation between phasors and space vectors in the positive- and negative-sequence systems are

$$\dot{X}_+ = \boldsymbol{X}_+^{dq+} \quad \dot{X}_- = (\boldsymbol{X}_-^{dq-})^* \tag{59}$$

VII. References

[1] "Fault current contributions from wind plants," 2015 68th Annual Conference for Protective Relay Engineers, College Station, TX, 2015, pp. 137-227.

[2] K. W. Jones, P. Pourbeik, G. Kobet et al, "Impact of Inverter Based Generation on Bulk Power System Dynamics and Short-Circuit Performance," Task Force on Short-Circuit and System Performance Impact of Inverter Based Generation, Tech. Rep. PES-TR68, July. 2018.

[3] A. K. Elnaggar, J. L. Rueda and I. Erlich, "Comparison of short-circuit current contribution of Doubly-Fed induction generator based wind turbines and synchronous generator," *2013 IEEE Grenoble Conference*, Grenoble, 2013, pp. 1-6.

[4] M. Nagpal, M. Jensen, M. Higginson et al, "Protection Challenges and Practices for Interconnecting Inverter Based Resources to Utility Transmission Systems," Tech. Rep. PES-TR81, July. 2020.

[5] A. Haddadi, M. Zhao, I. Kocar, U. Karaagac, K. W. Chan and E. Farantatos, "Impact of Inverter-Based Resources on Negative Sequence Quantities-Based Protection Elements," in *IEEE Transactions on Power Delivery*, vol. 36, no. 1, pp. 289-298, Feb. 2021.

[6] Y. Chang, M. Zhao and I. Kocar, "The Impact of DFIG Control Schemes on Negative-Sequence based Differential Protection Elements," in *Electric Power Systems Research*, vol. 211, no. 108564, Oct. 2022.

[7] K. El-Arroudi and G. Joós, "Performance of Interconnection Protection Based on Distance Relaying for Wind Power Distributed Generation," in *IEEE Transactions on Power Delivery*, vol. 33, no. 2, pp. 620-629, April 2018.

[8] Y. Chang, J. Hu, G. Song, X. Kong and Y. Yuan, "Impact of DFIG-based wind turbine's fault current on distance relay during symmetrical faults," in *IET Renewable Power Generation*, vol. 14, no. 66, pp. 3097-3102, Dec. 2020.

[9] R. Gagnon et al., "Hydro-Québec Strategy to Evaluate Electrical Transients Following Wind Power Plant Integration in the Gaspésie Transmission System," in *IEEE Transactions on Sustainable Energy*, vol. 3, no. 4, pp. 880-889, Oct. 2012.

[10] G. Li et al., "DFIG-based wind farm electromagnetic dynamic model and impact on protection relay of transmission network," *2011 International Conference on Advanced Power System Automation and Protection*, Beijing, 2011, pp. 694-698.

[11] U. Karaagac, H. Saad, J. Peralta, and J. Mahseredjian, "Doubly-fed induction generator based wind park models in EMTP-RV," Polytech. Montreal, Internal rep., Apr. 2016.

[12] WECC Second Generation Wind Turbine Models, January 23, 2014 https://www.wecc.biz/Reliability/WECC-Second-Generation-Wind-Turbine-Models-012314.pdf.

[13] IEC 61400-27-1. Electrical simulation models - Wind turbines, International Electrotechnical Commission Std., Rev. Edition 1, February 2015.

[14] X. He and H. Geng, "An overview on wind farm modelling for power system stability studies," *8th Renewable Power Generation Conference (RPG 2019)*, Shanghai, China, 2019, pp. 1-8.

[15] IEC 60909-0:2016, Short-circuit currents in three-phase A.C. systems-Part 0: Calculation of currents. International Electrotechnical Commission, 2016.

[16] F. Jimenez-Buendia, A. Honrubia-Escribano, A. Lorenzo-Bonache, E. Artigao-Andicoberry and E. Gomez-Lazaro, "Short-Circuit Current Contribution of Doubly-Fed Wind Turbines according to IEC and IEEE Standards," in *IEEE Transactions on Power Delivery*, vol. 36, no. 5, pp. 2904-2912, Oct. 2021.

[17] L. V. Strezoski and M. D. Prica, "Short-circuit analysis in large-scale distribution systems with high penetration of distributed generators," in *IEEE/CAA Journal of Automatica Sinica*, vol. 4, no. 2, pp. 243-251, 2017.

[18] D. F. Howard, J. Liang and R. G. Harley, "Short-Circuit Modeling of DFIGs With Uninterrupted Control," in *IEEE Journal of Emerging and Selected Topics in Power Electronics*, vol. 2, no. 1, pp. 47-57, March 2014.

[19] T. Kauffmann, U. Karaagac, I. Kocar, S. Jensen, J. Mahseredjian and E. Farantatos, "An Accurate Type III Wind Turbine Generator Short Circuit Model for Protection Applications," in *IEEE Transactions on Power Delivery*, vol. 32, no. 6, pp. 2370-2379, Dec. 2017.

[20] A. Haddadi, I. Kocar, T. Kauffmann, U. Karaagac, E. Farantatos and J. Mahseredjian, "Field validation of generic wind park models using fault records," in *Journal of Modern Power Systems and Clean Energy*, vol. 7, no. 4, pp. 826-836, July 2019.

[21] "Impact of Renewables on System Protection: Wind/PV Short-Circuit Phasor Model Library and Guidelines for System Protection Studies". Palo Alto, CA: EPRI, 2016.

[22] E. ON. Netz. GmbH, "Grid Code - High and Extra High Voltage," Bayreuth, Germany, April 2006.

[23] "Technical rule for connecting wind farm to power system," GB/T 19963-2011, 2011.

[24] R. Teodorescu; M. Liserre; P. Rodriguez, "Grid Converter Control for WTS," in *Grid Converters for Photovoltaic and Wind Power Systems* , IEEE, 2007, pp.205-236.

[25] L. Xu, "Enhanced Control and Operation of DFIG-Based Wind Farms During Network Unbalance," in *IEEE Transactions on Energy Conversion*, vol. 23, no. 4, pp. 1073-1081, Dec. 2008.

[26] J. Hu, H. Xu and Y. He, "Coordinated Control of DFIG's RSC and GSC Under Generalized Unbalanced and Distorted Grid Voltage Conditions," in *IEEE Transactions on Industrial Electronics*, vol. 60, no. 7, pp. 2808-2819, July 2013.

[27] VDE, "VDE-AR-N 4120: Technical requirements for the connection and operation of customer installations to the high-voltage network (TCC high-voltage)," 2015.

[28] Technical Specification for Connecting Wind Farm to Power System—Part 1: On Shore Wind Power, GB/T 19963.1-2021, 2021.

[29] "IEEE Standard for Interconnection and Interoperability of Inverter-Based Resources (IBRs) Interconnecting with Associated Transmission Electric Power Systems," in *IEEE Std 2800-2022*, vol., no., pp.1-180, 22 April 2022.

[30] Y. Chang, I. Kocar, J. Hu, U. Karaagac, K. W. Chan and J. Mahseredjian, "Coordinated Control of DFIG Converters to Comply with Reactive Current Requirements in Emerging Grid Codes," in *Journal of Modern Power Systems and Clean Energy*, vol. 10, no. 2, pp. 502-514, March 2022.

[31] G. Abad, J. Lopez, M. A. Rodriguez, L. Marroyo, and G. Iwanski, "Steady State of the Doubly Fed Induction Machine," in *Doubly Fed Induction Machine: Modeling and Control for Wind Energy Generation Applications*, 1, Wiley-IEEE Press, 2011, pp.155-208.

[32] D. Zhu, X. Zou, L. Deng, Q. Huang, S. Zhou and Y. Kang, "Inductance-emulating control for DFIG-based wind turbine to ride-through grid faults," *IEEE Transactions on Power Electronics*, vol. 32, no. 11, pp. 8514-8525, Nov. 2017.

[33] X. Zou, D. Zhu, J. Hu, S. Zhou and Y. Kang, "Mechanism Analysis of the Required Rotor Current and Voltage for DFIG-Based WTs to Ride-Through Severe Symmetrical Grid Faults," *IEEE Trans. Power Electronics*, vol. 33, no. 9, pp. 7300-7304, Sep. 2018.

[34] J. Mahseredjian, S. Dennetiére, L. Dubé, B. Khodabakhchian, and L. Gérin-Lajoie, "On a new approach for the simulation of transients in power systems," *Elect. Power Syst. Res*., vol. 77, no. 11, pp. 1514–1520, Sep. 2007.

[35] J.-S. Lacroix. "Multiphase Short-Circuit Analysis Solver in Phase Domain Using a Modified-Augmented-Nodal Analysis Approach", École Polytechnique de Montréal, 2012.

[36] L. Xu and Y. Wang, "Dynamic Modeling and Control of DFIG-Based Wind Turbines Under Unbalanced Network Conditions," in *IEEE Transactions on Power Systems*, vol. 22, no. 1, pp. 314-323, Feb. 2007.

[37] J. L. Blackburn, T. J. Domin, "Phasors and Polarity," in *Protective Relaying: Principle and Applications*, 4, CRC Press, 2014, pp.51-56.

[38] T. Kauffmann *et al*., "Short-Circuit Model for Type-IV Wind Turbine Generators With Decoupled Sequence Control," in *IEEE Transactions on Power Delivery*, vol. 34, no. 5, pp. 1998-2007, Oct. 2019.

[39] Y. Chang, J. Hu and X. Yuan, "Mechanism Analysis of DFIG-Based Wind Turbine's Fault Current During LVRT With Equivalent Inductances," in *IEEE Journal of Emerging and Selected Topics in Power Electronics*, vol. 8, no. 2, pp. 1515-1527, June 2020.

[40] Y. Chang, I. Kocar, J. Mahseredjian and U. Karaagac, "Analytical Characterization of DFIG Response to Asymmetrical Voltage Dips for Efficient Design," in *Electric Power Systems Research*, vol. 211, no. 108553, pp. 1-7, Oct. 2022.

[41] S. Engelhardt, J. Kretschmann, J. Fortmann, F. Shewarega, I. Erlich and T. Neumann, "Capability and limitations of DFIG based wind turbines concerning negative sequence control," *2013 IEEE Power & Energy Society General Meeting*, Vancouver, BC, Canada, 2013, pp. 1-5.

[42] V. R. F. B. De Souza, L. S. Barros, F. B. Costa and G. P. D. S. Junior, "Doubly Fed Induction Generator Low Voltage Ride Through Improvement Through Modular Multilevel Converter," *IEEE Access*, vol. 10, pp. 57914-57929, 2022.

[43] Z. Din, J. Zhang, Z. Xu, Y. Zhang and J. Zhao, "Low voltage and high voltage ride‐through technologies for doubly fed induction generator system: Comprehensive review and future trends," *IET Renewable Power Generation*, vol.15, no.3, pp.614, 2021.

[44] Ö. Göksu, R. Teodorescu, C. L. Bak, F. Iov and P. C. Kjær, "Instability of Wind Turbine Converters During Current Injection to Low Voltage

Grid Faults and PLL Frequency Based Stability Solution," in *IEEE Transactions on Power Systems*, vol. 29, no. 4, pp. 1683-1691, July 2014.

VIII. BIOGRAPHIES

Yuanzhu Chang (St. M'17-M'20) received the B.Eng. and Ph.D. degrees in Electronic Engineering (EE) from the School of Electrical and Electronic Engineering, Huazhong University of Science and Technology, China, in 2014 and 2020. Since 2020, he worked as a Postdoctoral Fellow at Polytechnique Montreal, University of Montreal, Quebec, Canada. He is currently a Postdoctoral Fellow at the Hong Kong Polytechnic University. His current research interests include fault analysis, fault ride through control and protective relaying of power systems. He received two best conference paper awards from IET. He serves as an Associate Editor for the PROTECTION AND CONTROL OF MODERN POWER SYSTEMS and was nominated as a Star Reviewer of IEEE TRANSACTIONS ON ENERGY CONVERSION for 2017-2018 and 2020.

Ilhan Kocar (SM'13) received the B.Sc. and M.Sc. degrees in EEE from Orta Doğu Teknik Üniversitesi, Ankara, Türkiye, in 1998 and 2003, respectively, and the Ph.D. degree in EE from École Polytechnique de Montréal (affiliated with Université de Montréal), QC, Canada, in 2009. He is currently a professor at the Hong Kong Polytechnic University. He has 20 years of experience with career highlights in research, development of computational tools for power system analysis, project engineering, and consulting. He is an associate editor of IEEE TRANSACTIONS ON POWER DELIVERY and JOURNAL OF MODERN POWER SYSTEMS AND CLEAN ENERGY.

Evangelos Farantatos (St. M'06-M'13-SM'18) received the Diploma in Electrical and Computer Engineering from the National Technical University of Athens, Greece, in 2006 and the M.S. and Ph.D. degrees from the Georgia Institute of Technology, Atlanta, GA, USA, in 2009 and 2012, respectively. He is a Principal Project Manager with the Grid Operations and Planning R&D Group at EPRI, Palo Alto, CA. He is managing and leading the technical work of various R&D projects related to synchrophasor technology, power systems monitoring and control, power systems stability and dynamics, renewable energy resources modeling, grid operation with high levels of inverter-based resources and system protection. He is a Senior Member of IEEE. In summer 2009, he was an intern at MISO.

Aboutaleb Haddadi (St. M'11-M'15-SM'22) received the Ph.D. degree in electrical and computer engineering from McGill University, Montréal, QC, Canada, in 2015. From 2015 to 2020, he was a Postdoctoral Fellow and Research Associate with Polytechnique Montréal, Montréal, QC, Canada. Since 2020, he has been with the Electric Power Research Institute, Palo Alto CA, USA, as a Senior Engineer/Scientist and Technical Lead/Project Manager, where he leads R&D activities related to bulk system and distributed renewable energy resources modeling and system integration impacts. Dr. Haddadi is also the EPRI Manager of the Advanced Grid Innovation Lab for Energy (AGILe) of the New York Power Authority, White Plains, NY, USA. He is the chair of CIGRE working group C4.60 and is further active in a number of working groups of IEEE Power and Energy Society, Western Electricity Coordinating Council (WECC), and North American Electric Reliability Corporation (NERC). His research interests include renewable resource integration, power system protection, and power system modeling and simulation.

Manish Patel (M'04-SM'17) received his B.E. from B. V. M. Engineering College, V. V. Nagar, India in 2000 and Ph.D. from Clemson University, Clemson, SC in 2009, both in Electrical Engineering. He joined Georgia Power Company in 2006 as a Protection & Control Applications Engineer. Since then, he has spent 10 years in Protection & Control Applications and 6 years with Transmission Planning - Stability group. He is currently a Chief Engineer in the Protection & Control Applications department. He is an active member of the IEEE PSRC. He is a registered Professional Engineer in the state of Alabama.